Confusing head-on and precessing intermediate-mass binary black hole mergers

Juan Calderón Bustillo[1,2,3], Nicolas Sanchis-Gual[4], Alejandro Torres-Forné[5], and José A. Font[6,7]

[1] *Department of Physics, The Chinese University of Hong Kong, Shatin, N.T., Hong Kong*
[2] *Monash Centre for Astrophysics, School of Physics and Astronomy, Monash University, VIC 3800, Australia*
[3] *OzGrav: The ARC Centre of Excellence for Gravitational-Wave Discovery, Clayton, VIC 3800, Australia*
[4] *Centro de Astrofísica e Gravitação - CENTRA, Departamento de Física, Instituto Superior Técnico - IST, Universidade de Lisboa - UL, Avenida Rovisco Pais 1, 1049-001, Portugal*
[5] *Max Planck Institute for Gravitational Physics (Albert Einstein Institute), Am Mühlenberg 1, Potsdam 14476, Germany*
[6] *Departamento de Astronomía y Astrofísica, Universitat de València, Dr. Moliner 50, 46100, Burjassot (València), Spain*
[7] *Observatori Astronòmic, Universitat de València, C/ Catedrático José Beltrán 2, 46980, Paterna (València), Spain*

We report a degeneracy between the gravitational-wave signals from quasi-circular precessing black-hole mergers and those from extremely eccentric mergers, namely head-on collisions. Performing model selection on numerically simulated signals of head-on collisions using models for quasi-circular binaries we find that, for signal-to-noise ratios consistent with Advanced LIGO observations, head-on mergers with total mass $M \in (130, 310) M_\odot$ would be identified as a precessing quasi-circular intermediate-mass black hole binary, located at a much larger distance. Ruling out the head-on scenario would require to perform model selection using currently nonexistent waveform models for head-on collisions, together with the application of astrophysically motivated priors on the (rare) occurrence of those events. We show that in situations where standard parameter inference of compact binaries may report component masses inside (outside) the pair-instability supernova gap, the true object may be a head-on merger with masses outside (inside) this gap. We briefly discuss the potential implications of these findings for the recent gravitational-wave detection GW190521.

Introduction. To date, the Advanced LIGO-Virgo gravitational-wave (GW) detector network [1, 2] has confirmed the observation of fifteen compact binary mergers [3–13], with further candidates being reported on a weekly basis. Some of these observations have represented milestones for GW astronomy and science itself. The GW events GW150914 [3] and GW170817 [10] implied respectively the first observation of a binary black hole (BBH) and a binary neutron star (BNS) merger while the event GW190814 is the first NS-BH candidate [14]. Recently, LIGO-Virgo announced GW190521: a short signal consistent with the merger of two massive BHs in a quasi-circular orbit with signatures of orbital precession located at a distance of $\simeq 5$ Gpc; which produced the first conclusively observed intermediate-mass BH (IMBH), with a mass of $\simeq 142 M_\odot$ [12, 13].

The component masses of GW190521 reside within the so-called pair-instability supernova (PISN) mass gap ($\sim 65 - 130 M_\odot$) predicted for the collapse of massive, low-metallicity stars [15]. Formation channels for BHs in the mass gap and above have been invoked in connection with PISN and pulsational PISN of progenitors with massive CO cores [16, 17] (see [18] for alternative proposals). Regardless of their formation, such collisions are the loudest sources for current detectors [19] and, as exemplified by GW190521, lead to remnant BH masses in the lower end of the IMBH range $\sim 100 - 250 M_\odot$.

Due to the low frequency of such signals, only the merger and ringdown yield significant power in the detector sensitive band, leaving a barely observable inspiral. Moreover, if the inspiral were completely out of band, it might be impossible to determine the formation channel of the remnant, making it unsafe to assume a standard quasi-circular BBH origin. If, however, a few inspiral cycles are visible in band, it may still be possible to determine this origin. For instance, such cycles would be strong for a non-precessing BBH while the modulations induced by a strongly precessing orbital plane can significantly suppress the inspiral right before merger [20, 21], causing a characteristic sine-Gaussian morphology. There are, however, alternative situations that may lead to such sine-Gaussian waveform, like hyperbolic encounters [22] and, as we will discuss, highly eccentric mergers.

Standard parameter estimation of the LIGO-Virgo BBH signals implements waveform templates for quasi-circular binaries with negligible eccentricity, as most formation scenarios predict that BBHs evolve in isolation for a long-enough time before they merge, efficiently circularizing the orbit via GW emission. Indeed, it has been shown that the eccentricity of all detections from the first two Advanced LIGO-Virgo observing runs is consistent with zero [23]. Nevertheless, highly eccentric BH mergers might occur in globular clusters through many-orbit, chaotic interactions of three or more BHs [24]. Other possible channels include dynamical interactions with an IMBH in the core of a globular cluster [25–27] or hyperbolic encounters between BHs in nuclear star clusters

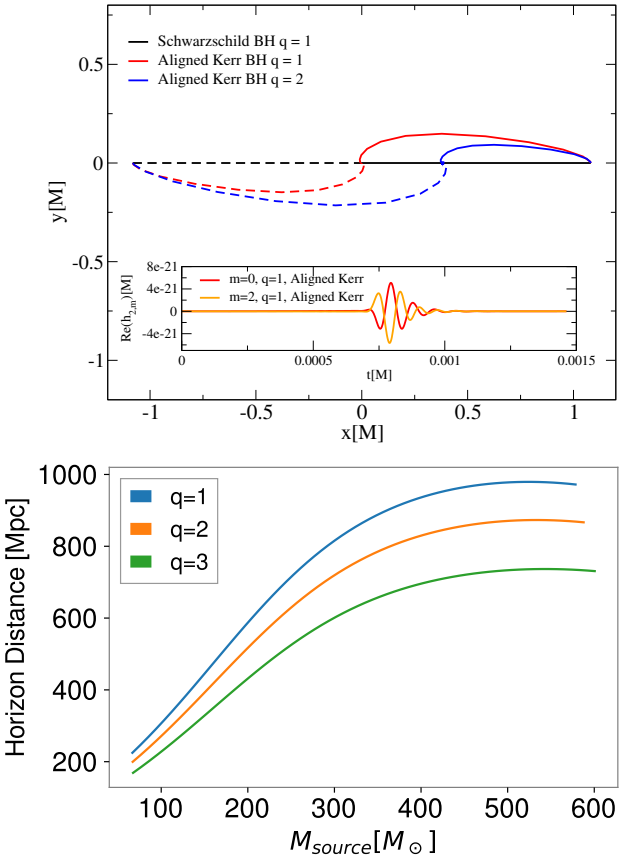

FIG. 1. Top: HOC trajectories for two Schwarzschild BHs and two Kerr BHs with different mass ratio and aligned spins a_1 and a_2 (see Table I). The BH spins induce a frame-dragging effect, curving the trajectories. Bottom: Average distance at which a HOC can produce a SNR of 12, using a triple detector network (LIGO Hanford-Livingston and Virgo) at design sensitivities.

[28, 29]. Detectability estimates of eccentric inspirals by the current network are provided in [30–32].

In this *Letter* we investigate whether similarities in the waveform morphology may lead to a confusion between precessing and extremely eccentric BBH mergers (head-on collisions; HOCs), discussing the astrophysical implications. We estimate the mass range and signal loudness in which such confusion might occur. We show that for masses $M \in [130, 310]M_\odot$ and signal-to-noise ratios (SNRs) typical among current observations, precessing BBH waveforms can be confused with HOC ones, producing a large over-estimation of the distance and a consequent under-estimation of the source-frame mass. Therefore, a HOC in this mass range would be genuinely identified as a precessing IMBH binary if only a quasi-circular merger scenario were considered. Remarkably, we find that if the HOC components are outside the PISN gap, parameter estimation with BBH waveforms may place one of the two masses inside it, reporting an apparent violation of the PISN gap.

$q = m_1/m_2$	a_1	a_2	D	$e_1^{\rm red}$	$e_2^{\rm red}$	$a_{\rm fin}$	$M_{\rm fin}/M_{\rm ini}$
1	0.58	0.58	2.34	0.14	0.14	0.35	0.999
2	0.60	0.56	2.34	0.09	0.20	0.39	0.999
3	0.61	0.55	2.34	0.06	0.23	0.43	0.999
1	0.00	0.00	2.34	0.00	0.00	0.00	0.999

TABLE I. Parameters of our simulations for head-on mergers: mass ratio (q), spins (a_i), separation (D), residual eccentricity ($e_i^{\rm red}$), final spin $a_{\rm fin}$, and mass loss ($M_{\rm fin}/M_{\rm ini}$).

Analysis. We perform parameter estimation on a family of numerically simulated signals from HOCs using two phenomenological waveform models for the inspiral-merger-ringdown of precessing and aligned-spin BBHs, respectively known as `IMRPhenomPv2` and `IMRPhenomD` [33–36] [1], and the parameter-estimation code `Bilby` [38, 39]. The numerical simulations of the HOCs and the GW extraction are performed with the `Einstein Toolkit` [40–42] using the `Cactus` framework with mesh refinement. The BBH initial data (Table I) are obtained from the `TwoPunctures` thorn [43] and we use the `MacLachlan` code [44] to solve Einstein's equations. Examples of the BBH trajectories and an illustrative GW strain signal are shown in the top panel of Fig. 1.

Our HOCs cover the total redshifted (detector-frame) mass range $M \in [100, 700]M_\odot$ related to the source-frame mass by $M = (1+z)M_{\rm source}$, with z the redshift. While the BBH emission is dominated by the quadrupole $(\ell, m) = (2, \pm 2)$ modes [45–47] the `IMRPhenom`, both the $(\ell, m) = (2, \pm 2)$ and $(\ell, m) = (2, \pm 0)$ are co-dominant for HOCs (see Fig. 1). Nevertheless, we place our HOCs face-on source to so that the HOC emission only includes the $(2, 2)$ mode, minimising waveform systematics.

We inject simulated signals from HOCs in zero noise, and use the standard likelihood for GW transients [48, 49]

$$\log \mathcal{L}(\theta|d) = -(d - h(\theta)|d - h(\theta))/2. \quad (1)$$

Here, d denotes our injection, $h(\theta)$ a BBH template h with source parameters θ, and $(a|b)$ the noise-weighted inner product [50],

$$(a|b) = 4\Re \int \frac{\tilde{a}(f)\tilde{b}^*(f)}{S_n(f)} df, \quad (2)$$

where $S_n(f)$ is the one-sided power spectral density of the detector. We consider a single Advanced LIGO detector working at design sensitivity [51] with a lower frequency cutoff of 20Hz. We characterise the loudness of our injections by the optimal SNR, $\rho_{\rm opt} = (h|h)^{1/2}$, inversely proportional to the luminosity distance D_L.

[1] We also performed another analysis using the model NRSur7dq4 [37]. However, this is limited to mass ratios $q \leq 4$, which caused our posteriors to rail against this limit.

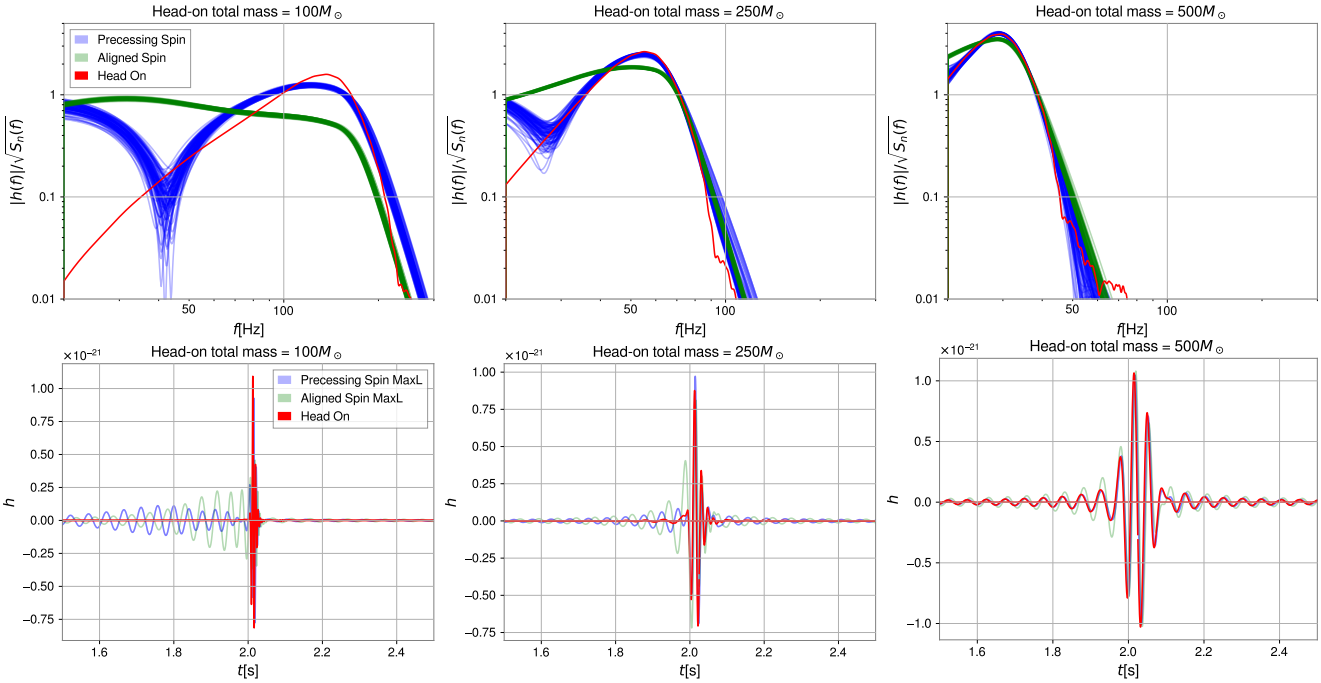

FIG. 2. Spectra and strain of HOCs and quasi-circular BBH mergers. Top: Amplitude of the Fourier transform of a $q = 2$ HOC injection (red) with varying total mass, together with that of the best-matching posterior samples for aligned-spin (green) and precessing (blue) quasi-circular binaries. Bottom: Corresponding strains band-passed between the lower and upper frequency cutoffs of our analysis $f \in [20, 512]$ Hz. As the total mass increases, the ringdowns predicted by the three waveform models become indistinguishable. This indicates that that all sources lead to the same final BH, and any differences are present only before merger.

The bottom panel of Fig. 1 shows the distance at which three of our initial data yield $\rho_{\rm opt} \geq 12$ across the Advanced LIGO-Virgo network working at its design sensitivity after averaging over inclination, sky-location, and polarisation angles. These distances are within reach of current BBH observations, so that these sources can in principle be detected.

We draw our attention to two main figures of merit. The first one is the ratio of the Bayesian evidence B for our precessing and non-precessing BBH models, $\log\beta = \log B(\chi_p) - \log B(\chi_p = 0)$. To compute the Bayesian evidence, we place flat priors on the detector-frame total mass and mass ratio parameters with ranges $M_{\rm tot} \in [10, 1000]M_\odot$ and $q \in [1, 5]$ and a spin prior with components uniformly distributed on the sphere. We use a prior on distance uniform in co-moving volume, a standard prior on source orientation and we fix the sky-location to the true one. The second figure of merit is the fitting factor (FF) [52] between the HOC waveforms and our BBH waveform models. We compute the FF as the fraction of SNR that the maximum likelihood (best fitting) template can recover from our injection with, using $\rho_{\rm opt} = 100$. A low FF indicates that the models miss an important fraction of the signal, leaving significant residuals in the data that would reveal that the signal is not a BBH. Instead, a large FF indicates that the signal is well reproduced by the BBH models and could be identified as a BBH by a matched-filter search [53–56]. These searches aim for FF=0.965 between the real signals and the templates [54, 55, 57]. We perform this analysis for optimal SNRs $\rho_{\rm opt} = (15, 25)$, consistent with the SNR of current detections [58].

Results. Fig. 2 shows the spectra of our $q = 2$ HOC injections, for three different masses, together with the best fitting waveforms for aligned-spin and precessing BBHs. Fig. 3 shows $\log\beta$ as a function of the detector-frame total mass of the HOC and the optimal SNR of the signal, for the $q = 2$ configuration. We also show the FF of both `IMRPhenomPv2` and `IMRPhenomD` to our injections. For all models we observe the following results. At the low-mass end (Fig. 2, left panels), when the full HOC signal is in band, none of the BBH models fits the data well, yielding FF below the detection threshold of 0.965 [54, 55]. For `IMRPhenomD`, the presence of strong inspiral cycles in the detector band at such low masses prevents BBH models from mimicking the absence of cycles in the HOC case. Something similar happens for `IMRPhenomPv2`, for which the suppression of the inspiral right before merger is preceded by unsuppressed cycles still visible in band. Conversely, at the high-mass end (Fig. 2, right panels), only the late ringdown HOC sig-

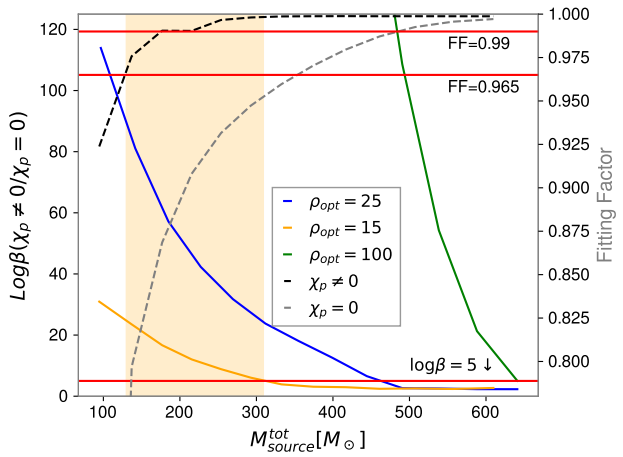

FIG. 3. Mass range (orange region) in which a $q = 2$ HOC can be confused with a precessing BBH merger. LogEvidence ratio $\log\beta$ (solid) for `IMRPhenomPv2` ($\chi_p \neq 0$) vs. `IMRPhenomD` ($\chi_p = 0$) and FF of each model (dashed, black and grey, respectively), as a function of total source-frame mass and optimal SNR of the injected HOC signal. Almost identical results are obtained for all cases in Table I.

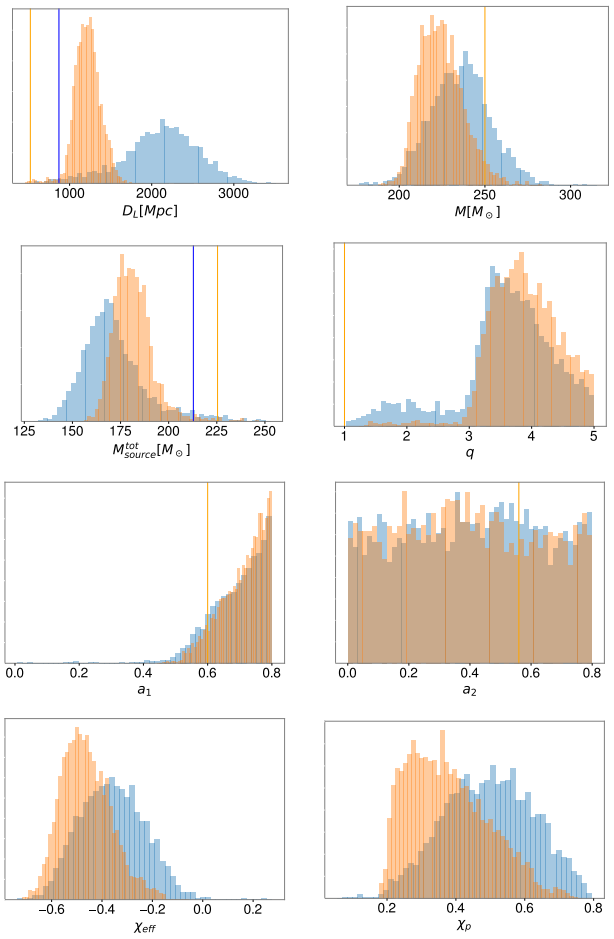

FIG. 4. Parameter recovery for our spinning $q = 1$ HOC injection using the quasi-circular precessing model `IMRPhenomPv2`. The true injection values are indicated by blue ($\rho_{\rm opt} = 15$) and orange (25) vertical lines. No true values are shown for $\chi_{\rm eff}$ and $\chi_{\rm p}$ as these are defined for quasi-circular binaries.

nal is in band so that both BBH models fit the injection with very high precision and no preference for any model is observed ($\log\beta < 5$).

As the mass of the source decreases, details of the early ringdown and merger signal that contain information about the HOC origin of the remnant become visible in band. While `IMRPhenomD` cannot mimic these details (as indicated by the fast decrease of its FF), `IMRPhenomPv2` fits the HOC signal perfectly down to $300M_\odot$, i.e. with FF=1. This leads to an increasing preference for `IMRPhenomPv2` for decreasing mass and increasing signal loudness.

For intermediate masses (orange region of Fig. 3) we find a range in which `IMRPhenomPv2` reaches FF well above the 0.965 threshold (reaching FF > 0.99 for $M > 250M_\odot$) while `IMRPhenomD` yields much lower values. The reason is that the strong modulation induced by precession suppresses the inspiral cycles before merger while the earlier inspiral cycles lie out of band (unlike what happens at lower masses). Hence, `IMRPhenomPv2` mimics the absence of inspiral cycles that characterises HOCs (Fig. 2, central panels). Therefore, the trigger would be detected by a search implementing precessing templates but not by current searches that implement aligned-spin templates [59]. (However, model-agnostic searches [60] might detect them [61].). On the other hand, the large $\log\beta$ would imply strong evidence for a precessing orbital plane under the assumption of a quasi-circular binary origin. For SNR=15 this might happen when the total source-frame mass is within $(130-310)M_\odot$ (orange region of Fig. 3).

Fig. 4 shows posterior parameter distributions for our spinning equal-mass HOC, recovered with `IMRPhenomPv2`. The signal is injected with $\rho_{\rm opt} = 15$ (blue) and 25 (orange) and we consider a total mass of $250M_\odot$ in the detector-frame. Again, we observe that the BBH model tries to mimic the HOC signal by pointing to a strongly precessing BBH (as indicated by the spin-precession parameter $\chi_{\rm p}$, which is zero for non-precessing systems [33, 62]). Remarkably, the posterior distribution of the primary spin hits the upper boundary of our prior. In addition, because BBHs are much more luminous than HOCs, the BBH model places the source ~ 3 times further away than it is. This, together with fair estimates of the detector-frame mass $M_{\rm det}$, leads to largely underestimated source-frame masses, $M_{\rm source} = M_{\rm det}/(1+z)$. Moreover, the large mass ratio q and

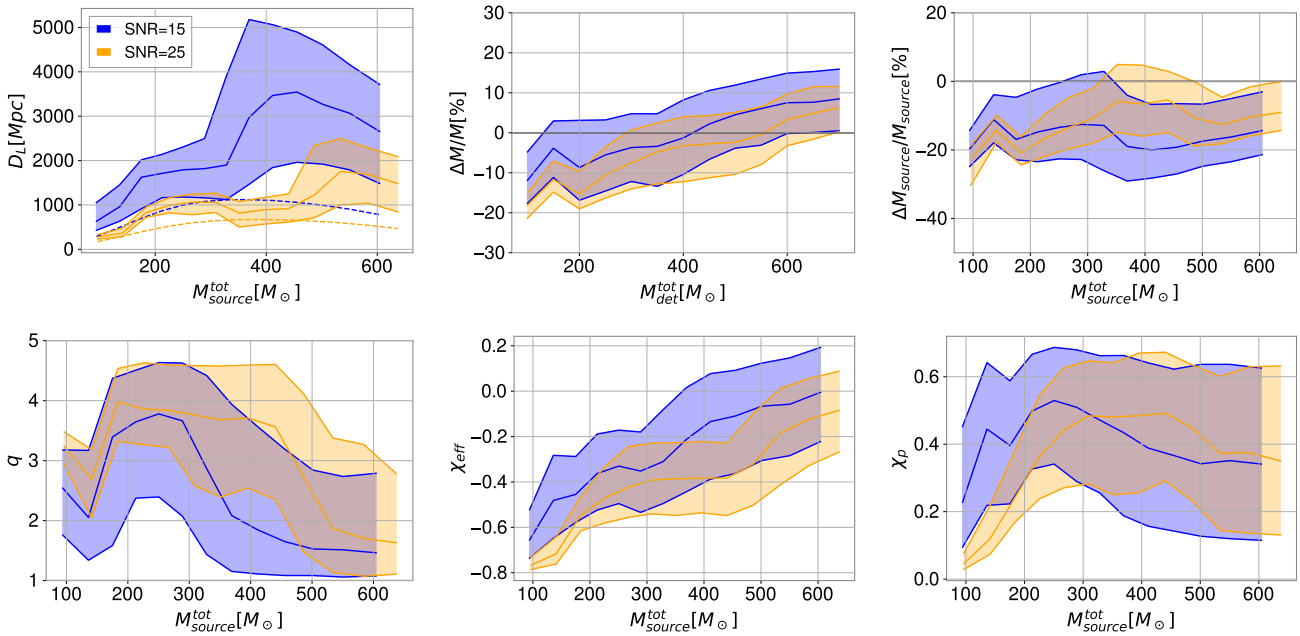

FIG. 5. Parameter recovery for our spinning $q = 1$ HOC injection, varying the total mass, and using the `IMRPhenomPv2` model for $\rho_{\rm opt} = 15$ (blue) and 25 (orange). The shaded contours represent 90% confidence intervals. For the luminosity distance the dashed lines represent the true values of the injection. Important biases toward large distances, large mass ratios, negative effective spins and strong precession are observed.

the negative effective-spin χ_{eff} [2], indicate that the BBH model tries to shorten the waveform as much as possible, to leave the low-frequency inspiral out of the detector band. The negative χ_{eff} is also a consequence of the low final spin of our binaries (see Table II), which the BBH tries to reach by having the BH spins anti-aligned with the angular momentum of the orbit.

Fig. 5 shows the posterior 90% confidence intervals on several parameters for the range of source-frame masses $\sim (100 - 650)M_\odot$. For the lowest masses, we observe results consistent with the ones previously described. For the largest masses, when only the ringdown is in band, the estimated detector-frame total mass is slightly overestimated. The reason may be that the BBH model has a larger likelihood for binaries with parameters that lead to the same remnant BH as the HOC. Since BBHs are more luminous, they require a slightly larger initial mass than the HOC to reach the same final BH. For all cases, the large overestimation of the source distance, combined with fair estimations of the detector-frame mass, consistently lead to a $\sim 20\%$ underestimation of the source-frame mass. In addition, the bias to large mass ratios leads to wrong estimates of the individual masses, whose implications we discuss next. These findings hold for all models of Table I.

Astrophysical implications. Fig. 6 shows 90% confidence intervals for the total and secondary source-frame masses of an equal-mass HOC, using `IMRPhenomPv2`. These two estimates are biased toward lower values, as a result of the biases found toward large distances and unequal masses. This has two main consequences.

First, for $\rho_{\rm opt} = 15$, HOCs in the narrow range $M_{\rm source} \in (130 - 135)M_\odot$ would have non-zero support for total measured masses below $100M_\odot$, preventing a conclusive detection of a remnant IMBH. While this is also true for lower masses, BBH waveforms would not fit HOC ones in this range, (see Figs. 2,3) making the quasi-circular BBH nature of the source easy to discard. Conversely, the measurement of an IMBH would be robust against the bias we describe.

Second, for certain range of component masses outside (inside) the PISN gap, precessing waveforms may report secondary mass estimates inside (outside) the gap. In particular, for an equal-mass HOC with $m_{1,\rm source} = m_{2,\rm source} \in (130, 250)M_\odot$ (above the gap), we recover posterior distributions for m_2 with strong support within the PISN gap. Since in this mass range BBH waveforms would fit well HOC ones, there would be no straightforward way to discard the BBH nature of the source. Yet, a strong preference for precession shall be flagged as a symptom that the source may be a HOC merger with masses outside the gap. For larger masses, for which

[2] $\chi_{\rm eff} = \frac{m_1\chi_1^{\parallel} + m_2\chi_1^{\parallel}}{m_1+m_2}$, with $\chi_i^{\parallel}$ being the component of the i-th spin along the orbital angular momentum

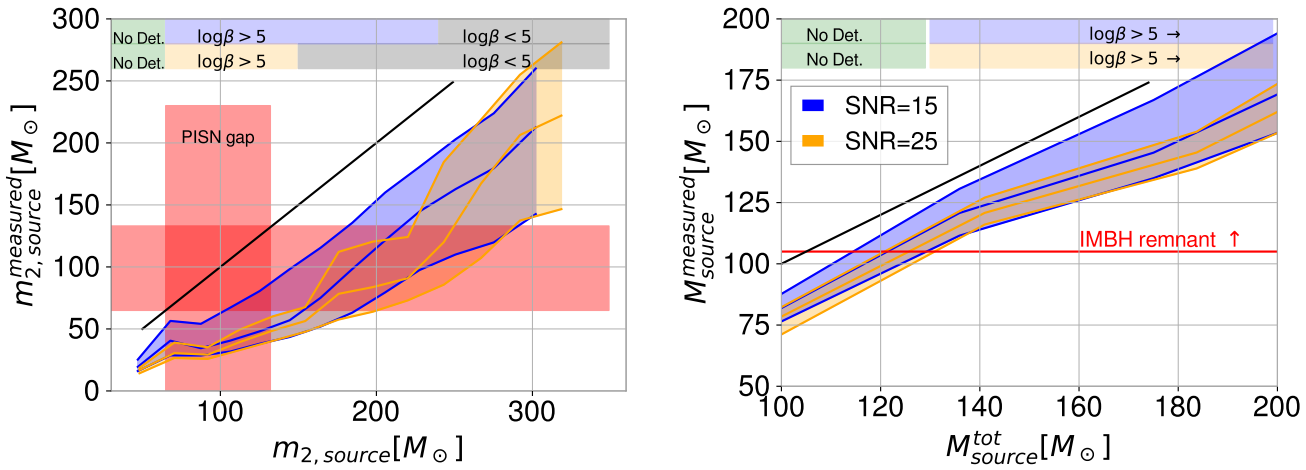

FIG. 6. 90% confidence intervals for the secondary mass (left) and total mass (right) of an equal-mass HOC, measured in the source-frame. The diagonal black line denotes "zero bias". The red regions enclose the boundaries of the PISN gap. The top blue and orange regions show the mass ranges in which the source may be confused with a precessing BBH, for $\rho_{\rm opt} = 15$ and 25, respectively. Top green regions display ranges in which BBH waveforms have a poor FF, so that the BBH nature of the source can be discarded. Top grey regions denote ranges in which `IMRPhenomD` and `IMRPhenomPv2` fit the head-on injection well enough that no model is preferred.

such preference would not occur (grey regions in Fig. 6) no such diagnose would be possible. Finally, when the source masses are in the interval $(65, 130)M_\odot$ (within the PISN gap), `IMRPhenomPv2` reports a secondary mass with no support within the gap.

Conclusions. GW signals from head-on BH collisions can be confused with those emitted by precessing quasi-circular BBH mergers. For a SNR=15, similar to that of GW190521, this confusion would happen when the head-on system has a total mass $M \in (130, 310)M_\odot$. In this interval, the absence of inspiral cycles characteristic of HOCs can be mimicked by the suppression of signal power right before merger induced by precession. Therefore, discerning between head-on and precessing scenarios would only be possible by performing model selection with currently unavailable models for HOCs and/or the placement of appropriate priors on the astrophysical probability of such collisions. The confusion brings significant biases in the source parameters. In particular, parameter estimation using templates for quasi-circular binaries would point to a highly precessing IMBH binary. Moreover, the distance would be overestimated by a factor of ∼3-4. the total, causing an underestimation of the source-frame mass by $10 - 20\%$, consequently biasing the component masses. In particular, HOCs with BH masses outside (inside) the PISN mass gap may be misinterpreted as BBHs with a component mass inside (outside) the gap, leading to a fake violation (compliance) of the PISN gap.

The recent GW observation GW190521 [12, 13] is a short signal with signatures of precession and component BHs in the PISN gap. Our results suggest that it may admit a head-on (or extremely eccentric) BBH interpretation. We note, however, that HOCs are not only much rarer than quasi-circular mergers but they would be further disfavoured if an uniform distribution of sources in the Universe is assumed, due to their intrinsic weakness. In addition, the remnant of GW150921 has an estimated spin $a_f = 0.72^{+0.10}_{-0.11}$, very difficult to obtain through HOCs of low mass ratio.

Nevertheless, given the recent claim of an associated electromagnetic counterpart to GW190521 located at a much shorter distance than estimated by quasi-circular BBH models [63], our results suggest that a highly eccentric merger (if not necessarily head-on) may reconcile both distance estimates.

Acknowledgements. We thank Paul D. Lasky, Simon Stevenson, and Nelson Christensen for comments on the manuscript. JCB is supported by the Australian Research Council Discovery Project DP180103155 and the Direct Grant, Project 4053406, from the Research Committee of the Chinese University of Hong Kong. NSG is supported by the Fundação para a Ciência e a Tecnologia (FCT) projects PTDC/FIS-OUT/28407/2017, UID/FIS/00099/2020 (CENTRA), and CERN/FIS-PAR/0027/2019. JAF is supported by the Spanish Agencia Estatal de Investigación (PGC2018-095984-B-I00) and by the Generalitat Valenciana (PROMETEO/2019/071). This work has further been supported by the European Union's Horizon 2020 research and innovation (RISE) programme H2020-MSCA-RISE-2017 Grant No. FunFiCO-777740. Parame-

ter estimation runs were done in the CIT Caltech cluster.

[1] J. Aasi et al. (LIGO Scientific Collaboration), Class. Quant. Grav. **32**, 074001 (2015), arXiv:1411.4547 [gr-qc].
[2] F. Acernese et al. (Virgo Collaboration), Class. Quant. Grav. **32**, 024001 (2015), arXiv:1408.3978 [gr-qc].
[3] B. P. Abbott et al. (Virgo, LIGO Scientific), Phys. Rev. Lett. **116**, 061102 (2016), arXiv:1602.03837 [gr-qc].
[4] B. Abbott et al. (Virgo, LIGO Scientific), Phys. Rev. Lett. **116**, 241103 (2016), arXiv:1606.04855 [gr-qc].
[5] B. P. Abbott, R. Abbott, T. D. Abbott, F. Acernese, K. Ackley, C. Adams, T. Adams, P. Addesso, R. X. Adhikari, V. B. Adya, C. Affeldt, M. Afrough, B. Agarwal, M. Agathos, K. Agatsuma, N. Aggarwal, O. D. Aguiar, L. Aiello, A. Ain, P. Ajith, B. Allen, G. Allen, A. Allocca, P. A. Altin, A. Amato, A. Ananyeva, S. B. Anderson, W. G. Anderson, S. Antier, S. Appert, K. Arai, M. C. Araya, J. S. Areeda, N. Arnaud, K. G. Arun, S. Ascenzi, G. Ashton, M. Ast, S. M. Aston, P. Astone, P. Aufmuth, C. Aulbert, K. AultONeal, and Avila-Alvarez (LIGO Scientific and Virgo Collaboration), Phys. Rev. Lett. **118**, 221101 (2017).
[6] B. P. Abbott et al. (Virgo, LIGO Scientific), Phys. Rev. Lett. **119**, 141101 (2017), arXiv:1709.09660 [gr-qc].
[7] B. P. Abbott et al. (Virgo, LIGO Scientific), Astrophys. J. **851**, L35 (2017), arXiv:1711.05578 [astro-ph.HE].
[8] B. Abbott et al. (LIGO Scientific, Virgo), Astrophys. J. Lett. **892**, L3 (2020), arXiv:2001.01761 [astro-ph.HE].
[9] (2020), arXiv:2004.08342 [astro-ph.HE].
[10] B. P. Abbott et al. (LIGO Scientific Collaboration, Virgo Collaboration), Phys. Rev. Lett. **119**, 161101 (2017), arXiv:1710.05832 [gr-qc].
[11] B. P. Abbott et al., The Astrophysical Journal **892**, L3 (2020).
[12] Abbott et al. (LIGO Scientific, Virgo), Physical Review Letters **125** (2020), 10.1103/PhysRevLett.125.101102.
[13] B. Abbott et al. (LIGO Scientific, Virgo), Astrophys. J. Lett. **900**, L13 (2020).
[14] R. Abbott et al., The Astrophysical Journal **896**, L44 (2020).
[15] A. Heger, C. L. Fryer, S. E. Woosley, N. Langer, and D. H. Hartmann, Astrophys. J. **591**, 288 (2003), arXiv:astro-ph/0212469 [astro-ph].
[16] S. E. Woosley, A. Heger, and T. A. Weaver, Reviews of Modern Physics **74**, 1015 (2002).
[17] H. Uchida, M. Shibata, K. Takahashi, and T. Yoshida, Phys. Rev. D **99**, 041302 (2019).
[18] U. N. Di Carlo, M. Mapelli, Y. Bouffanais, N. Giacobbo, S. Bressan, M. Spera, and F. Haardt, arXiv e-prints , arXiv:1911.01434 (2019), arXiv:1911.01434 [astro-ph.HE].
[19] B. P. Abbott et al. (Virgo, LIGO Scientific), Phys. Rev. **D96**, 022001 (2017), arXiv:1704.04628 [gr-qc].
[20] J. Healy, C. O. Lousto, J. Lange, R. O'Shaughnessy, Y. Zlochower, and M. Campanelli, Phys. Rev. D **100**, 024021 (2019), arXiv:1901.02553 [gr-qc].
[21] M. Boyle, D. Hemberger, D. A. B. Iozzo, G. Lovelace, S. Ossokine, H. P. Pfeiffer, M. A. Scheel, L. C. Stein, C. J. Woodford, A. B. Zimmerman, N. Afshari, K. Barkett, J. Blackman, K. Chatziioannou, T. Chu, N. Demos, N. Deppe, S. E. Field, N. L. Fischer, E. Foley, H. Fong, A. Garcia, M. Giesler, F. Hebert, I. Hinder, R. Katebi, H. Khan, L. E. Kidder, P. Kumar, K. Kuper, H. Lim, M. Okounkova, T. Ramirez, S. Rodriguez, H. R. Rüter, P. Schmidt, B. Szilagyi, S. A. Teukolsky, V. Varma, and M. Walker, arXiv e-prints , arXiv:1904.04831 (2019), arXiv:1904.04831 [gr-qc].
[22] R. Gold and B. Brügmann, Phys. Rev. D **88**, 064051 (2013), arXiv:1209.4085 [gr-qc].
[23] I. M. Romero-Shaw, P. D. Lasky, and E. Thrane, (2019), arXiv:1909.05466 [astro-ph.HE].
[24] M. Zevin, J. Samsing, C. Rodriguez, C.-J. Haster, and E. Ramirez-Ruiz, Astrophys. J. **871**, 91 (2019), arXiv:1810.00901 [astro-ph.HE].
[25] N. W. C. Leigh, N. Lützgendorf, A. M. Geller, T. J. Maccarone, C. Heinke, and A. Sesana, **444**, 29 (2014), arXiv:1407.4459 [astro-ph.SR].
[26] G. Fragione, I. Ginsburg, and B. Kocsis, Astrophys. J. **856**, 92 (2018), arXiv:1711.00483 [astro-ph.GA].
[27] G. Fragione and B. Kocsis, Phys. Rev. Lett. **121**, 161103 (2018), arXiv:1806.02351 [astro-ph.GA].
[28] R. M. O'Leary, B. Kocsis, and A. Loeb, **395**, 2127 (2009), arXiv:0807.2638 [astro-ph].
[29] B. Kocsis and J. Levin, Phys. Rev. D **85**, 123005 (2012), arXiv:1109.4170 [astro-ph.CO].
[30] J. Samsing, Phys. Rev. D **97**, 103014 (2018), arXiv:1711.07452 [astro-ph.HE].
[31] C. L. Rodriguez, P. Amaro-Seoane, S. Chatterjee, and F. A. Rasio, Phys. Rev. Lett. **120**, 151101 (2018), arXiv:1712.04937 [astro-ph.HE].
[32] M. E. Lower, E. Thrane, P. D. Lasky, and R. Smith, Phys. Rev. **D98**, 083028 (2018), arXiv:1806.05350 [astro-ph.HE].
[33] M. Hannam, P. Schmidt, A. Bohé, L. Haegel, S. Husa, F. Ohme, G. Pratten, and M. Pürrer, Phys. Rev. Lett. **113**, 151101 (2014), arXiv:1308.3271 [gr-qc].
[34] P. Schmidt, M. Hannam, and S. Husa, Phys. Rev. **D86**, 104063 (2012), arXiv:1207.3088 [gr-qc].
[35] S. Khan, S. Husa, M. Hannam, F. Ohme, M. Pürrer, X. Jiménez Forteza, and A. Bohé, Phys. Rev. D **93**, 044007 (2016), arXiv:1508.07253 [gr-qc].
[36] S. Husa, S. Khan, M. Hannam, M. Pürrer, F. Ohme, X. Jiménez Forteza, and A. Bohé, Phys. Rev. D **93**, 044006 (2016), arXiv:1508.07250 [gr-qc].
[37] V. Varma, S. E. Field, M. A. Scheel, J. Blackman, D. Gerosa, L. C. Stein, L. E. Kidder, and H. P. Pfeiffer, Physical Review Research **1** (2019), 10.1103/physrevresearch.1.033015.
[38] G. Ashton et al., Astrophys. J. Suppl. **241**, 27 (2019), arXiv:1811.02042 [astro-ph.IM].
[39] I. M. Romero-Shaw et al., "Bayesian inference for compact binary coalescences with bilby: Validation and application to the first ligo–virgo gravitational-wave transient catalogue," (2020), arXiv:2006.00714.
[40] F. Loffler et al., Class. Quant. Grav. **29**, 115001 (2012), arXiv:1111.3344 [gr-qc].
[41] "Einstein toolkit:http://www.einsteintoolkit.org,".
[42] M. Zilhão and F. Löffler, International Journal of Modern Physics A **28**, 1340014 (2013).
[43] M. Ansorg, B. Bruegmann, and W. Tichy, Phys. Rev. **D70**, 064011 (2004), arXiv:gr-qc/0404056.
[44] J. D. Brown, P. Diener, O. Sarbach, E. Schnetter, and M. Tiglio, Phys. Rev. D **79**, 044023 (2009), arXiv:0809.3533 [gr-qc].

[45] J. Calderón Bustillo, P. Laguna, and D. Shoemaker, Phys. Rev. **D95**, 104038 (2017), arXiv:1612.02340 [gr-qc].

[46] C. Capano, Y. Pan, and A. Buonanno, Phys.Rev. **D89**, 102003 (2014), arXiv:1311.1286 [gr-qc].

[47] J. Calderón Bustillo, F. Salemi, T. Dal Canton, and K. P. Jani, Phys. Rev. **D97**, 024016 (2018), arXiv:1711.02009 [gr-qc].

[48] L. S. Finn, Physical Review D **46**, 5236 (1992).

[49] J. D. Romano and N. J. Cornish, Living Reviews in Relativity **20** (2017), 10.1007/s41114-017-0004-1.

[50] C. Cutler and E. E. Flanagan, Phys. Rev. **D49**, 2658 (1994), arXiv:gr-qc/9402014 [gr-qc].

[51] D. Shoemaker et al. (LIGO Scientific Collaboration), LIGO-T0900288, https://dcc.ligo.org/cgi-bin/DocDB/ShowDocument?docid=2974 (2010).

[52] T. Apostolatos, Phys.Rev. **D52**, 605 (1995).

[53] B. Allen, W. G. Anderson, P. R. Brady, D. A. Brown, and J. D. E. Creighton, Phys. Rev. **D85**, 122006 (2012), arXiv:gr-qc/0509116 [gr-qc].

[54] S. A. Usman et al., Class. Quant. Grav. **33**, 215004 (2016), arXiv:1508.02357 [gr-qc].

[55] T. Dal Canton and I. W. Harry, (2017), arXiv:1705.01845 [gr-qc].

[56] C. Messick et al., Phys. Rev. D **95**, 042001 (2017), arXiv:1604.04324 [astro-ph.IM].

[57] S. M. Privitera, "The importance of spin for observing gravitational waves from coalescing compact binaries with ligo and virgo.".

[58] B. P. Abbott et al. (LIGO Scientific, Virgo), (2018), arXiv:1811.12907 [astro-ph.HE].

[59] I. Harry, S. Privitera, A. Bohé, and A. Buonanno, Phys. Rev. **D94**, 024012 (2016), arXiv:1603.02444 [gr-qc].

[60] S. Klimenko et al., Phys. Rev. D **93**, 042004 (2016), arXiv:1511.05999 [gr-qc].

[61] K. Chandra, G. V., J. C. Bustillo, and A. Pai, (2020), arXiv:2002.10666 [astro-ph.CO].

[62] P. Schmidt, F. Ohme, and M. Hannam, Phys. Rev. **D91**, 024043 (2015), arXiv:1408.1810 [gr-qc].

[63] M. Graham, K. Ford, B. McKernan, N. Ross, D. Stern, K. Burdge, M. Coughlin, S. Djorgovski, A. Drake, D. Duev, M. Kasliwal, A. Mahabal, S. van Velzen, J. Belecki, E. Bellm, R. Burruss, S. Cenko, V. Cunningham, G. Helou, S. Kulkarni, F. Masci, T. Prince, D. Reiley, H. Rodriguez, B. Rusholme, R. Smith, and M. Soumagnac, Physical Review Letters **124** (2020), 10.1103/physrevlett.124.251102.